MICROSTRUCTURE AND MARTENSITIC TRANSFORMATION OF SELECTIVE LASER MELTED NiTi SHAPE MEMORY ALLOY PARTS

CARLO A. BIFFI[*], JACOPO FIOCCHI [†], PAOLA BASSANI[ϒ] AND AUSONIO TUISSI[Ψ]

[*] National Research Council Institute of Condensed Matter Chemistry and Technologies for Energy, Unit of Lecco, CNR ICMATE; Via Previati 1/E, 23900 Lecco, Italy.
e-mail: carloalberto.biffi@cnr.it

[†] National Research Council Institute of Condensed Matter Chemistry and Technologies for Energy, Unit of Lecco, CNR ICMATE; Via Previati 1/E, 23900 Lecco, Italy.
e-mail: jacopo.fiocchi@icmate.cnr.it

[ϒ] National Research Council Institute of Condensed Matter Chemistry and Technologies for Energy, Unit of Lecco, CNR ICMATE; Via Previati 1/E, 23900 Lecco, Italy.
e-mail: paola.bassani@cnr.it

[Ψ] National Research Council Institute of Condensed Matter Chemistry and Technologies for Energy, Unit of Lecco, CNR ICMATE; Via Previati 1/E, 23900 Lecco, Italy.
e-mail: ausonio.tuissi@cnr.it

Key words: Niti, Shape Memory Alloy, Additive Manufacturing, Selective Laser Melting, Microstructure, Martensitic Transformation.

Abstract.

Additive Manufacturing allows to design and realize 3D parts, integrating additional functionalities offered by the interaction between complex shapes and the material properties. Results can be even more appealing when functional materials, like Shape Memory Alloys, are printed: new opportunities for smart devices can be opened.

In the present bulk and lattice structures of Nitinol were additively manufactured with a Seletive Laser Melting. A pulsed laser, which is more suitable for manufacturing thin parts, was selected to process the initial powder. The selection of the process parameters, like laser power and exposure time, was performed for maximizing the relative density. Furthermore, the microstructure and the martensitic transformation temperatures were analyzed through X-rays diffraction and differential scanning calorimetry, respectively. A comparison between the initial powder and SLMed parts was also considered. Finally, the mechanical properties of Niti builts under compression were tested for both bulk and lattice structures.

1 INTRODUCTION

Among smart and functional materials, Shape Memory Alloys (SMAs) are well known, thanks to their unique properties, namely shape memory effect (SME) and pseudoelasticity (PE) [1]. Quasi-equiatomic NiTi compound is the most diffused SMAs for their stable and optimal functional properties. These properties depend on a solid to solid phase transformation, indicated as martensitic transformation (MT), which can be found in Ti rich-NiTi and Ni rich-NiTi alloys above or below room temperature, respectively. This permits to determine the use of these materials as actuators or for biomedical devices, according with the implementation of the SME or PE, respectively.

The operating temperatures of the MT is of relevant importance for the specific application. Anyways, these are affected strongly by Ni/Ti ratio, the manufacturing of the NiTi SMAs is very challenging for getting stable functional characteristics [2].

In the recent years, the use of Additive Manufacturing (AM) techniques for realizing 3D parts in NiTinol is becoming an attractive solution for advanced devices [3-5]. The manufacturing of Nitinol using different AM technologies, like selective laser melting (SLM), electron beam melting (EBM) and direct energy deposition (DED), has been studied in several experimental works [6-8]. Anyways, among the AM methods the SLM process is the most diffused one and nowadays it can offer the best performances and compositional control, which is fundamental for this system. In fact, the MT and the related functional properties of SLM built Nitinol parts have been shown to be almost comparable to those of the wrought alloy [9-11]. The compositional issue remains an aspect to be controlled during the laser process in order to allow the Ni/Ti ratio [12-13]. Moreover, the SLMed microstructure can be strongly textured, depending of the process conditions, and this can be optimized for enhancing the functional response of NiTinol parts [14].

It is demonstrated that the heat transfer during SLM, particularly the laser emission mode, can affected the microstructure and the corresponding mechanical properties [15] in AlSi based alloys. Moreover, it was even found that the relative density and the geometric features can be affected by the laser emission modes: continuous wave (CW) or pulsed wave (PW) [16]. In fact, it is reported that a CW laser is preferable for producing fully dense large parts, while PW is more suitable for thin and precise structures. These results can be supported by previous works regarding some experiments using CW and PW lasers in welding, too [17].

As in literature the SLM process has been studied for printing Nitinol samples only by means of CW lasers, in the present work the feasibility of SLM with a PW laser was investigated in the view of realizing thin parts in Nitinol, in which more gentile energies are deposited on the powder bed for the local melting.

2 EXPERIMENTAL

Bulk and lattice samples were produced from quasi equiatomic NiTi powder (see Figure 1a) by means of a SLM system (mod. AM400 from Renishaw), equipped with a pulsed wave laser. The process parameters, listed in Table 1, were used for manufacturing cylinders (5 mm

in height and 3 mm in diameter) printed on a Ti6Al4V platform. Full factorial design was performed for fixing the optimal set of process parameters able to maximize the relative density. Moreover, selected process parameters, reported in Table 2, were used for printing lattice structures (10 mm x 100 mm x 30 mm), whose schematic is depicted in Figure 1b. The schematics of the scanning strategies, used for printing the cylinders and lattice parts, are shown in Figure 2, respectively.

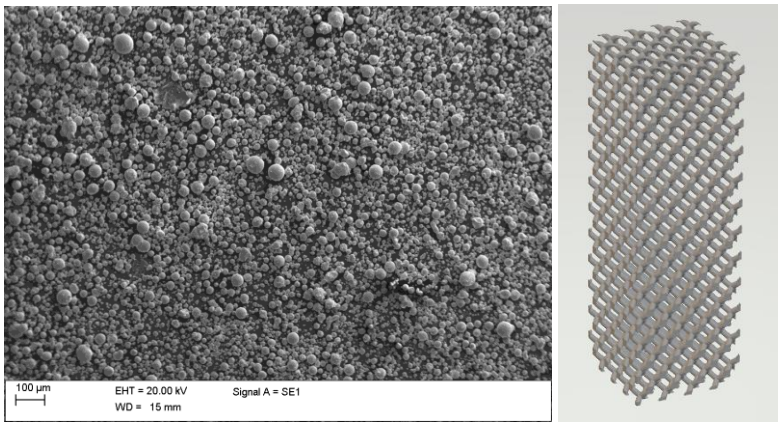

(a) (b)

Figure 1: Nitinol powder used for the SLM printing (a) and schematic of the lattice structure (b).

Table 1: List of variable and fixed process parameters used for printing NiTi cylinders

Parameters	Values
Power	50-75-100-125-150 W
Exposition time	25-50-75-100 µs
Scanning strategy	Meander
Atmosphere	Argon
Layer thickness	30 µm
Hatch distance	50 µm
Point distance	50 µm
Laser spot size	65 µm

Table 2: List of process parameters used for printing NiTi lattice structure

Parameters	Values
Power	75 W
Exposition time	75 µs
Scanning strategy	Contour
Atmosphere	Argon
Layer thickness	30 µm
Hatch distance	50 µm
Point distance	50 µm
Laser spot size	65 µm

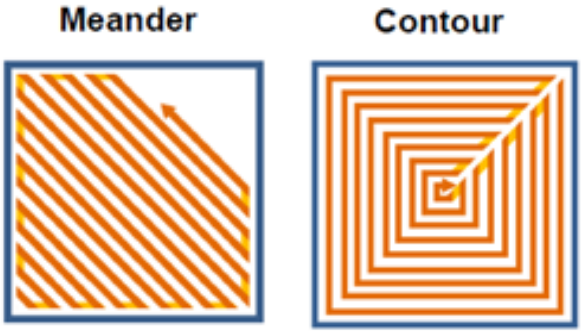

(a) (b)

Figure 2: Schematic of the scanning strategies, used for printing the cylinders and lattice parts, respectively: meander (a) and contour (b).

The cylinders, in as built condition, were characterized according to the following features : (i) relative density with the Archimede's method; (ii) martensitic transformation via differential scanning calorimetry (DSC) ; (iii) microstructure via X-rays diffraction (XRD); and (iv) superelasticity via compression testing. As term of comparison, the characteristic features of the initial powder were studied and compared to the ones of the as built samples. Moreover, the lattice, in as built condition, were studied according to DSC and compression testing.

In details, relative density measurements were performed with a Gibertini E 50 S/2 balance as set up for implementing the Archimedes method. Calorimetric properties of the SLMed Niti samples were investigated through a differential scanning calorimeter (DSC, mod. SSC 5200 by Seiko Instruments), in the [-100°C; 150°C] range with heating/cooling rate of 10°C min. Characteristic temperatures and corresponding transformation enthalpies were evaluated for both direct/reverse transformations upon cooling/heating scans respectively. XRD spectra were collected by a diffractometer (Panalytical X'Pert Pro) using Cu Kα radiation operating at 40 kV and 30 mA on the samples' xy surfaces in the 20-70° 2theta range; the measurements were performed using a spinner at 30°C. Compressive tests were conducted at room temperature by means of an MTS 2/M machine, equipped with extensometer, at strain rate of 0.01 min^{-1}. 8 complete loading and unloading cycles, up to 10% in strain, were carried out on cylindrical and lattice samples.

3 ANALYSIS OF RESULTS AND DISCUSSION

3.1 Evaluation of the feasibility window

According with the PW emission mode in SLM process, the energy density per unit of volume, F, namely fluence, was calculated as follows:

$$F = \frac{P \cdot t_{exp}}{d_p \cdot d_h \cdot s} \quad (1)$$

where P, t_{exp}, d_p, d_h and s indicate laser power, exposition time, point distance, hatch distance and layer thickness, respectively. The schematic of the temporal and spatial distribution of the laser pulses is shown in Figure 3.

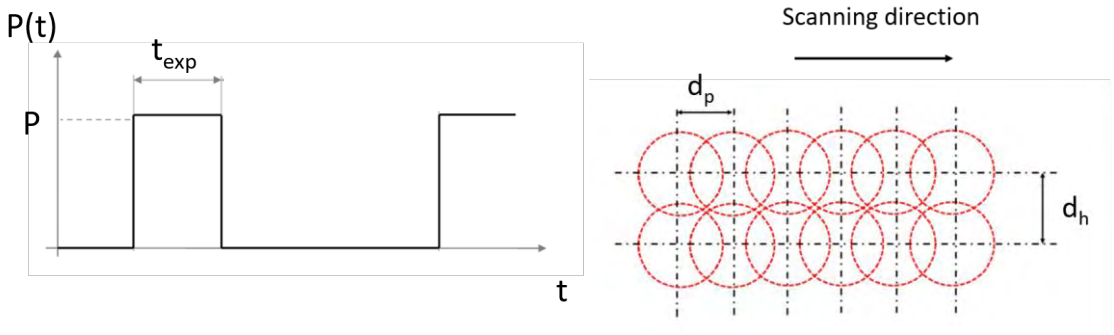

(a) (b)

Figure 3: Schematic of the temporal power profile and spatial pulses path (b) in SLM performed with PW emission mode [17].

The identification of the feasibility window has been performed considering the main process parameters (power and exposition time), representative of the PW emission mode, aimed at the maximization of the relative density. Figure 4 shows the correlation between the relative density, measured with the Archimede's method, and the energy density.

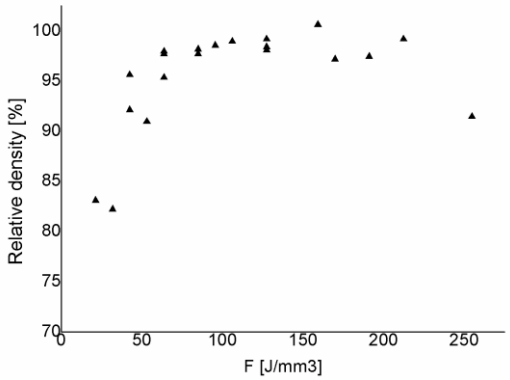

Figure 4: Evolution of the relative density as function of the energy density F.

The evolution of relative density as function of the energy density is coherent with what is reported in literature: density first steeply increases up to a peak, and then decreases more gradually. It is noteworthy that the peak of density for the different exposure time values occurs for higher energy densities with increasing exposure time. The highest relative density value, is achieved with laser power of 125 W and exposure time of 75 µs.

3.2 Martensitic transformation, microstructure and mechanical behaviour of massive Nitinol samples

In Figure 5 the DSC scans of the sample, obtained with the process condition previously selected for maximizing the relative density, and the initial powder, are shown. A unique peak can be detected upon heating, while two peaks, characteristics of the transformation from austenite to R phase, and from R phase to martensite, are visible upon cooling. The SLMed sample, in as built condition, shows the peaks of the MT upon heating and cooling at temperatures, which are pretty lower to the ones of the Nitinol powder, probably due to the presence of internal stresses. The transformation enthalpies are almost constant, indicating that the amount of material involved in the MT is maintained after the SLM process: about 7 J/g and 9 J/g are the heats exchanged during the direct and reverse MT for both the SLMed sample and initial powder.

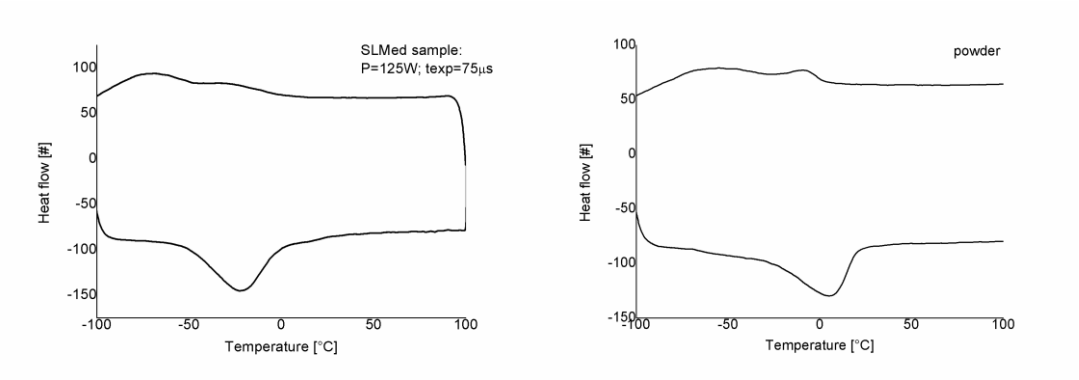

(a) (b)

Figure 5: DSC scans of the NiTinol cylindrical sample, realized in the process condition: P=125W; texp=75 μs (a); Nitinol powder (b).

In Figure 6 the XRD patterns, acquired at room temperature, of the SLMed sample and the initial powder, are shown. XRD spectrum of the SLMed sample indicates that the principal phase is austenite (B2). This is in good agreement with the DSC scan shown in Figure 5a. However, other peaks, related to residual martensite (B19'), could be found, too. On the contrary, the initial powder is fully characterized by austenite (see Figure 6b). Moreover, the shape of the peaks is quite different: as in the SLMed sample, broader peaks with lower intensity are present, if compared to the Nitinol powder. The broadening effect of the peaks and the presence of martensite can be due to different microstructures, associated to cooling rates faster in SLM than in the powder production, and to residual stresses, respectively.

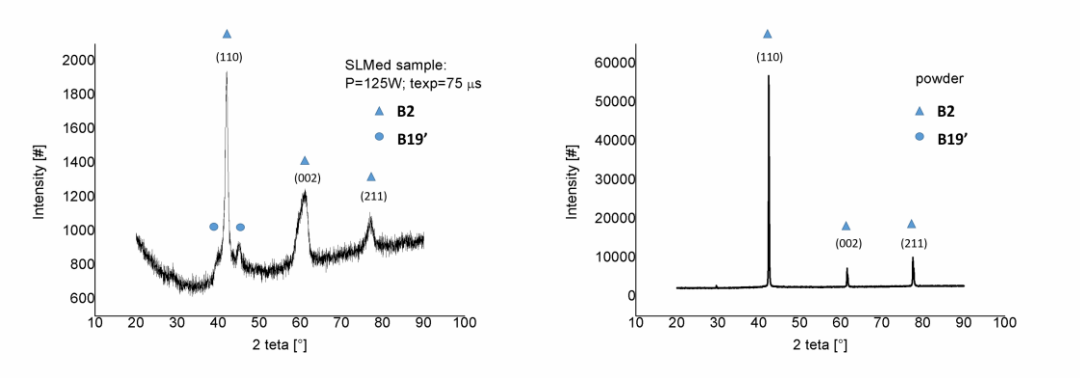

(a) (b)

Figure 6: XRD patterns of the NiTinol cylindrical sample, realized in the process condition: P=125W; texp=75μs (a); Nitinol powder (b).

In Figure 7 the stress-strain behavior of the SLMed sample, obtained by mechanical testing at room temperature in compression configuration, is shown. Here, some loading/unloading cycles, characterized by increasing the applied strain, were performed in order to analyze the PE. The sample does not exhibit a complete recovery of the applied strain at room temperature. An evident PE behavior is visible, according to the majority of recoverable strain up to 6% in correspondence of the last cycle, with a residual strain of 1%. Anyways, a flag like behavior was not observed.

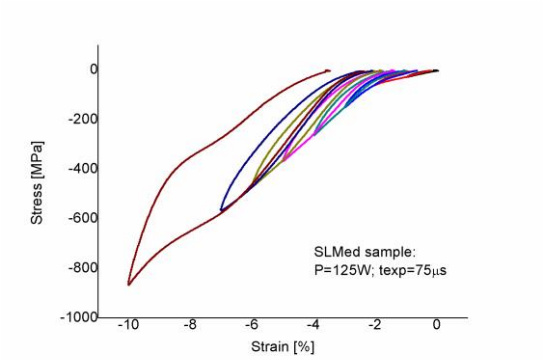

Figure 7: Mechanical cycling under compression of the NiTinol cylindrical sample.

3.3 Martensitic transformation and mechanical behavior of Nitinol lattice structures

In this paragraph the characterization of the Nitinol lattice structures is reported. In Figure 8 some lattice structures are shown. The process parameters were slightly varied with respect to the ones used for the massive samples because generally lower energy density is required for building thinner structures. The martensitic transformation of the lattice part is

depicted in the DSC scan, reported in Figure 9. The main difference among the lattice part and the other samples, characterized in Figure 5, is the one step MT upon heating and cooling. Table 3 summaries the transformation temperatures and enthalpies of the SLMed samples in both massive and lattice configurations, and the powder. The variability of the enthalpies of the direct (indicated as ΔH_{dir}) and reverse (indicated as ΔH_{rev}) processes is quite limited: 6-7 J/g and 8-10 J/g, respectively. This indicates that the amount of material involved in the MT remains almost unvaried by the SLM process. On the contrary, the transformation temperatures are more affected by the process. Particularly, the lattice structure shows a broadening of the MT peaks. Due to the energy density being lower in the lattice structure than in the massive samples, it appears reasonable that Ni evaporation, usually present during laser processing, is not the reason of the temperatures shift. On the contrary, residual stresses can be more probably the cause of the modification of the peaks of the MT. In fact, the geometry of the lattice structure printed in this work (see Figure 1b and Figure 8) is characterized by thin struts, linked each other in several points of joining at limited distances: this may provoke the formation of intense values of residual stresses, which could be relaxed after proper heat treatments. This aspect will be analyzed in future works.

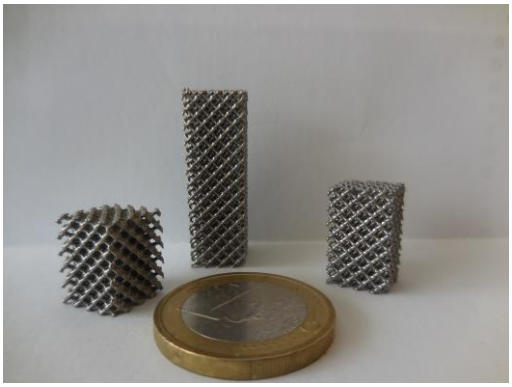

Figure 8: Picture of the NiTinol lattice structures, realized in the process condition: P=75W; texp=75µs.

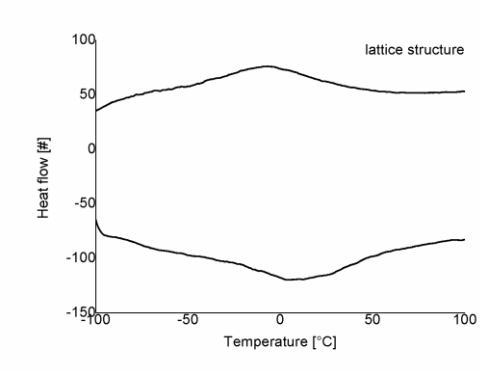

Figure 9: DSC scans of the NiTinol lattice structure, realized in the process condition: P=75W; texp=75µs.

Table 3: Characteristic temperatures and transformation enthalpies of massive sample, lattice structure and initial Nitinol powder.

Samples	ΔH_{dir} [J/g]	R_s [°C]	M_f [°C]	ΔH_{rev} [J/g]	A_s [°C]	A_f [°C]
Massive sample	6.3	7	-97	9.8	-53	1
Lattice structure	7.5	44	-52	10.5	-47	76
Powder	7.0	3	-94	8.1	-34	19

According with the measurement of the A_f temperature from the DSC scan of Figure 9, the mechanical response of the lattice structure can be affected by the presence of both austenite and martensite, due to the uncomplete reverse MT at room temperature. Figure 10 shows the mechanical cycling behavior under compression of the lattice sample, evaluated at room temperature. After an initial elastic part, the curves are characterized by a flat plateau, which shall be ascribed to the densification process typical of trabecular structures. A limited pseudoelastic behavior is evident, presumably because of the presence of martensite in the sample, as evidenced by DSC analyses. Measured stresses, computed considering the nominal section of the whole structure, are sensibly lower than the ones typical of bulk samples because of the large void areas that characterize the lattice part. Moreover, it shall be considered that the deformation mechanism involves bending of the struts, thus further reducing the apparent strength. The large area subtended by the loading-unloading curves, higher than the one displayed by bulk parts, confirms the ability of the lattice structure of absorbing high energy during deformation.

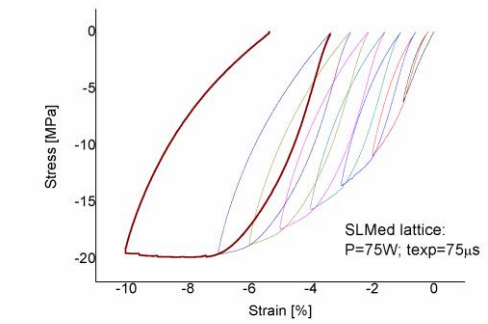

Figure 10: Mechanical cycling under compression of the NiTinol lattice structure.

4 CONCLUSIONS

In the present work the feasibility of Selective Laser Melting process of Nitinol samples, using a pulsed wave emission mode for emitting the laser power, was studied.

According to the selection of the best combination between laser power and exposition time, almost full dense samples can be obtained. Further characterizations were performed on the as built sample produced in this optimized process condition. The martensitic transformation is exhibited in the as built condition, without any post heat treatment, with enthalpies comparable to the powder and transformation temperatures just decreased. The microstructure of the printed sample, analyzed at room temperature via XRD measurements, indicates the presence of martensite, probably induced by residual stresses. Mechanical testing under compression indicates a PE behaviour at room temperature, showing a recoverable strain up to 6% in correspondence of a residual strain of 1%.

Additionally to the manufacturing and characterization of massive samples, lattice structures, representative of thin elements, were successfully printed with selected process parameters. For the lattice samples the martensitic transformation varied significantly from the initial powder and the SLMed massive samples, probably more due to residual stresses than to potential compositional modifications. The mechanical properties are also very interesting, as both PE and energy absorption contributes are present, thanks to the integration of functional performances of Nitinol and deformability and ductility of lattice structures within the same part.

ACKNOWLEDGEMENTS

The authors would like to acknowledge Nicola Bennato from CNR ICMATE for assisting during the experiments.

REFERENCES

[1] H. Funakubo, *Shape Memory Alloys*, Gordon and Breach Science Publishers, Amsterdam, (1987).

[2] M. Nishida, C. Wayman, T. Honma, Precipitation processes in near-equiatomic TiNi shape memory alloys, *Metallurgical Transactions A* (1986) **17**:1505-1515.

[3] Elahinia, M., Shayesteh Moghaddam, N., Taheri Andani, M., Amerinatanzi, A., Bimber, B. A., & Hamilton, R. F. Fabrication of NiTi through additive manufacturing: A review. *Progress in Materials Science* (2016) **83**:630-663.

[4] Van Humbeeck J. Additive Manufacturing of Shape Memory Alloys, *Shape Memory and Superelasticity*, (2018) **4-2**:309-312.

[5] S. Dadbakhsh, M. Speirs, J. Van Humbeck, J.-P. Kruth, Laser additive manufacturing of bulk and porous shape memory NiTi alloys: from processes to potential biomedical applications, *MRS Bulletin* (2016) 765-7774.

[6] C. Wang, X.P. Tan, Z. Du, S. Chandra, Z. Sun, C.W.J. Lim, S.B. Tor, C.S. Lim, C.H. Wong, Additive manufacturing of NiTi shape memory alloys using pre-mixed powders, *Journal of Materials Processing Technology* (2019) **271**:152-161.

[7] Quan Zhou, Muhammad Dilawer Hayat, Gang Chen, Song Cai, Xuanhui Qu, Huiping Tang, Peng Cao, Selective electron beam melting of NiTi: Microstructure, phase transformation and mechanical properties, *Materials Science and Engineering A* (2019) **744**:290-298.

[8] Reginald F. Hamilton, Beth A. Bimber, Todd A. Palmer, Correlating microstructure and

superelasticity of directed energy deposition additive manufactured Ni-rich NiTi alloys, *Journal of Alloys and Compounds* (2018) **739**:712-722.

[9] S. Saedi, N. S. Moghaddam, A. Amerinatanzi, M. Elahinia, H.E. Karaca, On the effects of selective laser melting process parameters on microstructure and thermomechanical response of Ni-rich NiTi, *Acta Materialia* (2018) **14**:552-560.

[10] M. Speirs, X. Wang, S. Van Baelen, A. Ahadi, S. Dadbakhsh, J.P. Kruth, J. Van Humbeck, On the Transformation Behavior of NiTi Shape-Memory Alloy Produced by SLM, *Shape Memory and Superelasticity* (2016) **2-4**:310.

[11] S. Saedi, A.S. Turabi, M.T. Andani, C. Haberland, H.Karaca, M. Elahinia, The influence of heat treatment on the thermomechanical response of Ni-rich NiTi alloys manufactured by selective laser melting, *Journal of Alloys and Compounds* (2016) **677:**204-210.

[12] S. Shiva, I.A. Palani, S.K. Mishra, C.P. Paul, L.M. Kukreja, Investigation on the influence of composition in the development of Ni-Ti shape memory alloy using laser based additive manufacturing, *Optics and Laser Technology* (2015) **69**:44-51.

[13] M. Mahmoudi, G. Tapia, B. Franco, J. Ma, R. Arroyave, I. Karaman, A. Elwany, On the printability and transformation behavior of nickel-titanium shape memory alloys fabricated using laser powder-bed fusion additive manufacturing, *Journal of Manufacturing Processes* (2018) **35:**672-680.

[14] T. Bormann, B. Muller, M. Schinhammer, A. Kessler, P. Thalmann, M. de Wild, Microstructure of selective laser melted nickel-titanium, *Materials Characterization* (2014) **94:**189-202.

[15] C.A. Biffi, J. Fiocchi, P. Bassani, A. Tuissi, Continuous wave vs pulsed wave laser emission in selective laser melting of AlSi10Mg parts with industrial optimized process parameters: Microstructure and mechanical behaviour, *Additive Manufacturing* (2018) **24:**639-646.

[16] A.G. Demir, P. Colombo, B. Previtali, From pulsed to continuous wave emission in SLM with contemporary fiber laser sources: effect of temporal and spatial pulse overlap in part quality, *Int. J. Adv. Manuf. Technol.* (2017) 1–14.

[17] E. Assuncao, V. Williams, Comparison of continuos wave and pulsed wave laser welding effects, *Opt. Lasers Eng.* (2013) **51**:674–680.

[18] M.T. Andani, S. Saedi, A. S. Turabi, M.R. Karamooz, C. Haberland, H.E. Karaca, M. Elahinia, Mechanical and Shape Memory properties of porous Ni50.1Ti49.9 alloys manufactured by selective laser melting, *Journal of the mechanical behavior of biomedical materials* (2017) **68**:224–231.